JOURNAL OF SPACECRAFT AND ROCKETS
Vol. 39, No. 3, May–June 2002

Engineering Notes

ENGINEERING NOTES are short manuscripts describing new developments or important results of a preliminary nature. These Notes cannot exceed six manuscript pages and three figures; a page of text may be substituted for a figure and vice versa. After informal review by the editors, they may be published within a few months of the date of receipt. Style requirements are the same as for regular contributions (see inside back cover).

Unsteady Separation in Flare-Induced Hypersonic Shock-Wave Boundary-Layer Interaction Flowfield

S. B. Verma* and G. Koppenwallner†
Hyperschall Technologie Göttingen,
37191 Katlenburg-Lindau, Germany

Introduction

THE shock-wave boundary-layer interaction (SWBLI) phenomenon represents a fundamental fluid dynamic problem that has been found to occur in a wide variety of high-speed flows, such as over forward-facing steps and compression ramps and past blunt fins and protuberances. As such, these flows find significant practical implications on aerodynamic control surfaces and in the propulsion systems of high-speed flight vehicles. Past studies have shown the interaction to be associated with unsteady behavior, which can generate severe surface pressure fluctuations. Under the influence of aerothermal effects, like those experienced during reentry, these fluctuating loads can pose significant problems to the successful flight of a high-speed aircraft.

The causes of unsteadiness of the shock wave,[1–3] particularly when the flow is separated, is one of the lesser known characteristics in SWBLI. Kistler[1] was perhaps the first to make fairly detailed high-frequency measurements in an attempt to characterize such unsteadiness, providing valuable quantitative data for flow over forward-facing steps in supersonic boundary layers. Later studies focused on the fluctuating wall pressure in the interaction regions of compression-ramp flowfields. Their results, although obtained from different flow geometries, exhibited statistical properties that were quite similar to those reported by Kistler.[1] Similar results have been obtained in three-dimensional flows, notably in those induced by blunt fins at supersonic speeds.[4] In these cases high-speed photography and wall-pressure fluctuation measurements have shown that large variations occur in the position and structure of the separation shock-wave system. Large-scale unsteadiness of the separation onset and reattachment regions has been observed[5] at hypersonic speed (Mach 7) in an interaction generated by a flare mounted concentrically on a cone-ogive cylinder model.

The primary focus of the present work is to investigate the phenomena of shock unsteadiness in a Mach 9 flare-generated SWBLI in more detail and to gain a better understanding of the mechanisms involved in their generation. For this reason laser schlieren system has been developed to analyze the fluctuating density flowfield above the model surface, which might be crucial in gaining insight of the various processes involved.[6] The flowfield was also analyzed using a conventional schlieren system and surface-pressure distributions. Further, evolution of energy content through the SWBLI and space-time correlations in the vicinity of separation point have been investigated.

Experimental Technique

Wind-Tunnel Facility and Test Model

The experiments were performed in the hypersonic wind tunnel at Hypersonic Technology Gottingen, a new facility developed on the Ludweig-tube principle.[7] This wind tunnel is an intermittent blowdown type with a test-section diameter of 250 mm and a variable Mach-number capability over the range of Mach 6–11 with maximum run time of 100 ms.

Figure 1a shows the schematic of the HALIS (High Alpha Inviscid Solution) Axisymmetric Configuration model (HAC), an axisymmetric geometry based on the Space Transportation System (STS) orbiter (space shuttle) that was used to provide the interaction test surface. In this model configuration the curvature, shown as "expansion region," just upstream of the flare is an important part of the orbiters geometry. The slight expansion experienced by the flow in this region tends to reduce any compression as a result of a separation shock and might also play a major role in real-gas effects for the viscous-interaction region. Although the HAC profile does incorporate essential features of the orbiter, it does not duplicate the orbiter's geometry exactly (e.g., the scaled flare length on the HAC is much longer then the flap length on the orbiter). The model has been manufactured in aluminum on a computer numerical control (CNC) machine with an accuracy of ± 0.02 mm. Thereafter, the model surface was polished with a mean roughness of 0.8 μm.

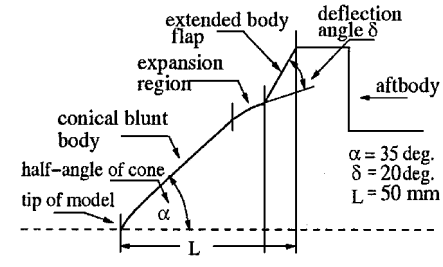

Fig. 1a Schematic of the HAC model.

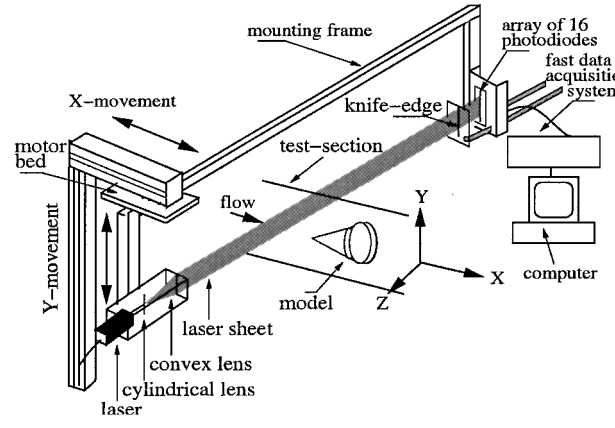

Fig. 1b Schematic of the laser schlieren setup.

Received 28 August 2000; revision received 17 July 2001; accepted for publication 18 July 2001.

*Humboldt Fellow; currently Research Scientist, Space Propulsion, DLR Lampoldshausen, D-74239 Hardthausen, Germany; shashi.verma@dlr.de.
†Head, Aerodynamics Division, Max-Planck Strasse 19.

The test-section Mach number (M_∞) for the present experiments was $9.68 \pm 4\%$ and was calculated using the measured stagnation pressure on the model nosetip and Rayleigh's pitot-tube formula. Tests were conducted for a charge tube pressure of $50 \pm 1.2\%$ bar, which results in a test-section stagnation pressure (P_0) of $42.25 \pm 1\%$ bar. To avoid condensation of the relieved flow in the nozzle, the gas column that is ejected during the shot is heated to 773 ± 0.2 K, resulting in a test-section stagnation temperature (T_0) of 738 ± 0.2 K. The corresponding freestream Reynolds number (Re) per unit length for the test condition was 6.072×10^6 m^{-1}. The boundary-layer state upstream of separation was laminar.

Pressure measurements on the HAC model surface were made using differential-type pressure transducers that were not mounted flush to the surface but placed in the model support sting downstream of the model. The pressure taps on the model surface are connected to these transducers via rubber tubes. The transducers were calibrated before each test run. The error in pressure measurements for all of the surface-pressure locations was approximately $\pm 3\%$ of the mean pressure.

A data-acquisition system was used to record data for the present study. A 32-channel data-acquisition system was used to record data at a speed of up to 40 kHz. Data stored on the hard disk were available for postprocessing or graphical output. In addition, piezoresistive pressure gauges were calibrated and installed to measure the flow in the charge tube, test section, and vacuum tank.

Laser Schlieren System

Figure 1b shows the schematic of the laser schlieren setup. A parallel laser sheet is passed through the test section and projects on an array of 16 photodiodes placed on the opposite side of the test section. When the laser sheet passes an oscillatory shock, the diffracted light appears periodically, and a time trace obtained from the array of photodiodes shows unsteady voltage signals. This arrangement provides an idea of the existing density fluctuations in the flow and hence an insight to the fluctuating nature of flow. Because the response time of the photodiode is extremely small (4 ns), extremely high-frequency shock oscillations can be detected using this optical technique. Further, the arrangement can be moved to probe any section of flow, both horizontally and vertically. The arrangement is simple and more accessible than the quantitative schlieren or shadowgraph system. The instrument, however, was not calibrated against a known density gradient.

The system makes use of the index of refraction fluctuations to produce voltage signal fluctuations instead of absorption and scattering methods used earlier[8] and, therefore, seems to be more promising because 1) the sensitivity of the schlieren system can be adjusted to permit measurement of much smaller fluctuations than is possible with the other two systems and 2) the schlieren signals are more directly related to a property of the flow, that is, density.[8] The latter implies that the laser schlieren system provides voltage signals representative of the fluctuating density gradient flowfield.

Results and Discussion

Flow Visualization

Figure 2 shows the schlieren photos of the SWBLI flowfield on a HAC model with air as test gas. Initially, Fig. 2a, in addition to the main shock surrounding the HAC model, a small separation bubble can be seen along with a reattachment shock on the flare region. The next interval (Fig. 2b) shows the separation bubble to have significantly grown in size along with a backward movement of the reattachment shock on the flare. The separation shock is difficult to discern from the pictures. This seemingly random movement of the bubble causes the separation shock to oscillate, and because there exist large pressure gradients in the vicinity of the separation and reattachment locations, as seen in Fig. 3, which shows the surface-pressure distribution on the HAC model, such a motion will cause high fluctuating pressure levels to be generated. As such, the phenomena is of much concern and needs to be investigated in greater detail.

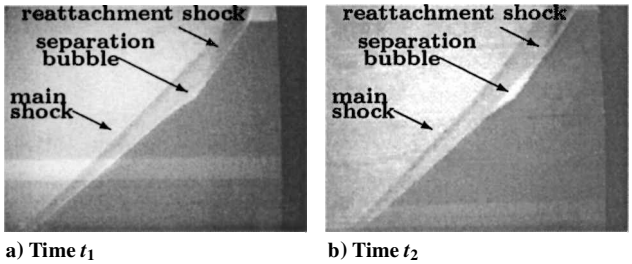

a) Time t_1 b) Time t_2

Fig. 2 Schlieren photographs of the HAC model at two time intervals with air as test gas; flow is from left to right.

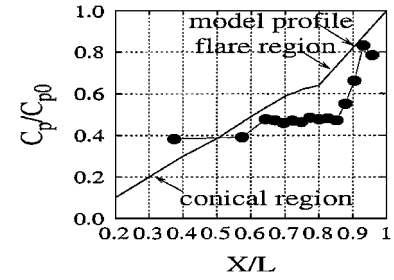

Fig. 3 Surface-pressure distribution on HAC model; the pressure measurements have been normalized first by the freestream dynamic pressure to obtain C_p then by the pressure coefficient at the stagnation point of the model C_{p0} for that run and time interval.

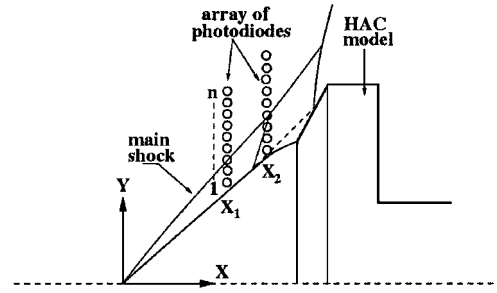

Fig. 4a Experimental procedure for laser schlieren flowfield analysis.

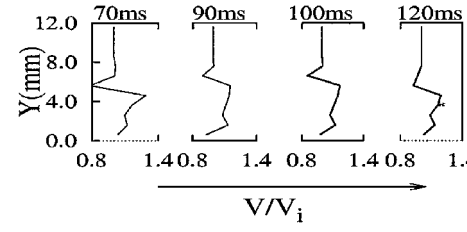

Fig. 4b Fluctuating density profiles normal to freestream direction as a function of time; $X/L = 0.80$.

Evolution of Energy Content

Figure 4a shows the experimental procedure for laser schlieren flowfield analysis, and Fig. 4b shows the fluctuating density gradient profiles obtained from an array of 12 active photodiodes at $X/L = 0.80$ (cone-flare junction). Care was exercised to keep the lowest photodiode 0.6 mm above the model surface. The voltage signal V (millivolts) from each channel is nondimensionalized by its initial value V_i (millivolts) at the beginning of flow. Further, because the knife edge is placed in the flow direction a decrease in voltage followed by an increase represents a shock. Away from the model surface, a single strong inflection point can be seen, which represents the main shock. Time-dependent profiles show an up-and-down motion of main shock indicating the existence of fluctuating separation bubble that displaces the main shock vertically in accordance with the change in its size. This characteristic was also observed in the schlieren pictures. The laser schlieren system, therefore, is capable of capturing the time-dependent characteristics during the interaction process.

Figure 5 presents the power spectra from the $P_0 = 50$ bar SWBLI at axial locations ranging from the undisturbed boundary layer to the end of the interaction process. The ordinate is the power spectral

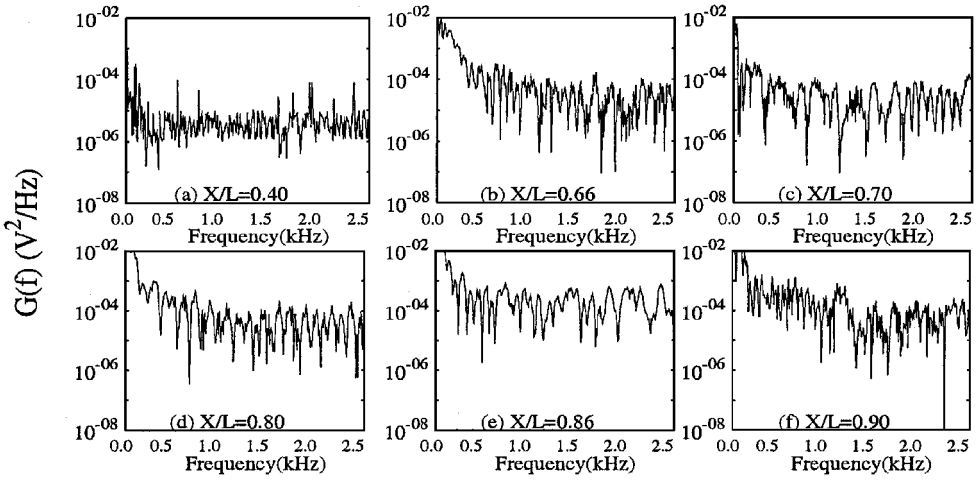

Fig. 5 Power spectra showing the evolution of energy content through the interaction; P_0 = 50 bar.

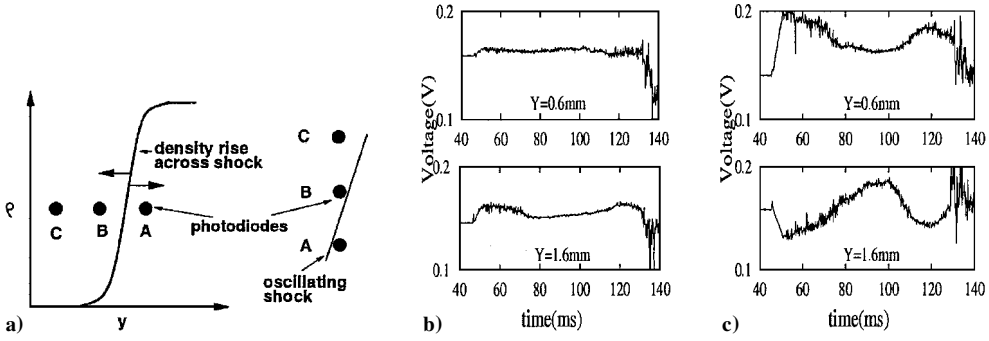

Fig. 6 Oscillating separation shock: a) two-point analysis; b) and c) simultaneous time traces of voltage signals (close to surface) near the separation region; P_0 = 50 bar; b) X/L = 0.40 and c) X/L = 0.66.

density function $G(f)$ in volts^2/hertz, and the abscissa is the frequency in kilohertz. The data are shown for the channels closest to the model surface (0.6 mm). The ordinate of these figures is the raw power spectral density plotted on logarithmic scale to more clearly illustrate the evolution of energy content of different frequency ranges through the interaction.[9] As expected, the incoming boundary-layer spectra are broadband with a very low energy content (Fig. 5a). As the separation point is approached (Fig. 5b), a significant increase in energy over the complete frequency range (especially in the low-frequency band) is observed. This change is thought to be caused by the motion of the separation shock. Farther downstream, (Fig. 5c), the spectrum shows a slight relaxation back to its original shape but with increased energy content over the entire range of frequency. At $X/L = 0.80$ the separation bubble has maximum thickness, and so the channel might be expected to be underneath the vortex core of the bubble. At this point (Fig. 5d) an increase in energy is observed in the frequency range of 0–1.0 kHz. This is followed by a simultaneous increase in strength of high-frequency fluctuations. As the reattachment point is approached $X/L = 0.86$ (Fig. 5e), a significant increase in energy of both low- and high-frequency fluctuations is observed, which is seen to be the maximum throughout the interaction process. This situation is likely because of the random fluctuation of the instantaneous position of reattachment shock and the reattaching of separated shear layer. Once this reattachment is accomplished, the spectrum at $X/L = 0.90$ (Fig. 5f) shows relaxation in energy of high-frequency fluctuations, but the higher energy in the low-frequency range still persists. Here the shape of the spectrum is more or less similar to that recorded near separation (Fig. 5b).

Unsteady Separation

From the preceding analysis we can conclude that the flow near separation is unsteady and that the increased energy levels near separation are caused by a random fluctuation in the instantaneous position of the separation shock. Past studies[2] reveal that the fluctuating separation shock generates intermittent wall-pressure signals. As a result, there exists large density as well as large pressure gradients in the vicinity of the separation point. A two-point analysis similar to that of Garg and Settles[9] and Willmarth et al.[10] was carried out with the present fluctuating density signal data. The locations of interest labeled as A, B, and C are shown in Fig. 6a. In this figure the ordinate is the flow density ρ in kilograms/meters^3, and the abscissa is the coordinate Y normal to freestream direction. Locations A and B indicate the photodiodes between which the separation shock oscillates while location C (neighboring B) lies away from the oscillating shock. When the shock oscillates, it crosses photodiode B at one time, and at the other, photodiode A. When the shock oscillates between two channels, the one that experiences an increase in density gradient (shock) shows a decrease in voltage signal, whereas the other shows an opposite behavior at that very instant. As such, the movement of the separation shock can be detected from the voltage signals of these two neighboring channels.

Figures 6b and 6c show the instantaneous time history of voltage signals at different axial locations near the separation point. Data are shown from first two channels closest to the model surface. It can be seen that voltage signals just upstream of separation (Fig. 6b) change in concert with one another, whereas those at separation (Fig. 6c) follow opposite trends, almost to the extent of mirror imaging. Figure 7 shows the simultaneous time history of voltage signals for photodiode channels that encounter the movement of of the main shock above the interaction, away from the model surface, and near the reattachment location. The behavior of the signals is similar to that observed near separation (Fig. 6c) and reveals that the motion of the separation and main shock are triggered by some common mechanism within the interaction regime causing the entire SWBLI flowfield to oscillate. A further observation from Figs. 6c, 7a, and 7b is that only relatively low-frequency fluctuations behave in this manner; high-frequency changes in the pressure signals do not necessarily follow the same trends. Thus, it can be inferred that the separation is associated with low-frequency fluctuations.

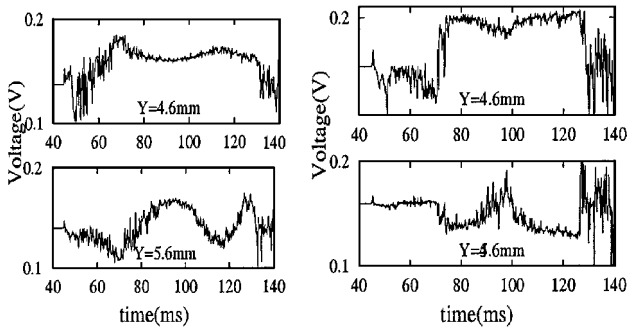

a) $X/L = 0.80$ b) $X/L = 0.86$

Fig. 7 Simultaneous time traces of voltage signals near the main shock region (above the bubble); P_0 = 50 bar.

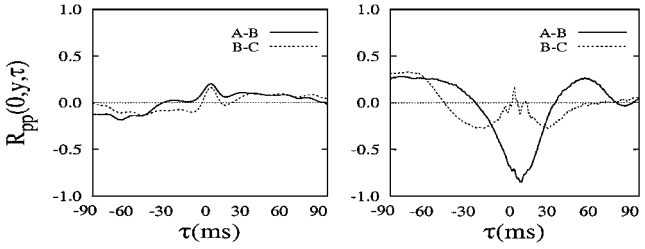

a) $X/L = 0.40$ b) $X/L = 0.66$

Fig. 8 Space-time correlation functions for photodiode locations (close to the surface) near the oscillating separation shock; P_0 = 50 bar.

Figure 8 shows the space-time correlation $R_{pp}(0, y, \tau)$ for channels separated in the Y direction, as a function of time delay τ (milliseconds) between the voltage signals from A and B and locations B and C. The point of interest is the value of the correlation at approximately zero time delay. Far upstream of separation (Fig. 8a) the plot shows a positive value for locations A–B and B–C. For axial locations $X/L = 0.40, 0.66$, A is $Y = 0.6$ mm from the surface, whereas B and C are $Y = 1.6$ and 2.6 mm, respectively, away from the surface. For downstream locations A is $Y = 1.6$ mm from surface, whereas B and C are $Y = 2.6$ and 3.6 mm, respectively, away from model surface. These distances were chosen wherever mirror imaging of signals from neighboring channels were observed and indicates that all locations experience similar density flow with the absence of any fluctuating density gradients. At separation (Fig. 8b) the space-time correlation value between these locations show opposite trends. Locations A and B (which are in close proximity to one another) show a large negative value, whereas B and C show a relatively large positive value indicating that, when photodiode A experiences a rise in density (as across a shock), the photodiode B experiences a fall and vice versa. Locations B and C experience a similar rise and fall of density.

Conclusions

The unsteadiness associated with the shock-wave boundary-layer interaction (SWBLI) flowfield on a HALIS axisymmetric configuration model is demonstrated in a Mach 9.68 flow with air as test gas. The SWBLI flowfield investigated generates high-pressure loads in the vicinity of separation and reattachment points. Near reattachment the pressure on the flare approaches the stagnation point pressure level. Off-surface flow study using the laser schlieren system revealed increased energy levels near the separation point suggesting random fluctuations in the instantaneous position of the separation shock. Space-time correlation of voltage signals from neighboring channels, exhibiting mirror-imaging effects, shows a negative value at zero time delay. The observation is consistent with the view that the separation shock translates back and forth, in response to the expansion and contraction motion of the separation bubble, in the vicinity of separation point on the HAC model, and hence is responsible for high-pressure loads at these locations.

References

[1]Kistler, A. L., "Fluctuating Wall Pressure Under a Separated Supersonic Flow," *Journal of the Acoustical Society of America*, Vol. 36, No. 3, 1964, pp. 543–550.

[2]Dolling, D. S., and Murphy, M. T., "Unsteadiness of the Separation Shock Wave Structure in a Supersonic Compression Ramp Field," *AIAA Journal*, Vol. 21, No. 12, 1983, pp. 1628–1634.

[3]Maull, D. J., "Hypersonic Flow over Axially Symmetric Spiked Bodies," *Journal of Fluid Mechanics*, Vol. 8, Pt. 4, 1969, pp. 584–592.

[4]Dolling, D. S., and Bogdonoff, S. M., "An Experimental Investigation of the Unsteady Behaviour of Blunt Fin-Induced Shock Wave Turbulent Boundary layer Interaction," AIAA Paper 81-1287, June 1981.

[5]Horstman, C. C., and Owen, F. K., "New Diagnostic Technique for the Study of Turbulent Boundary Layer Separation," *AIAA Journal*, Vol. 12, No. 10, 1974, pp. 1436–1438.

[6]Verma, S. B., and Koppenwallner, G., "Experimental Study of Shock Unsteadiness on an Hyperboloid Model Using Laser Schlieren," *9th AG-STAB Workshop*, edited by H. J. Heinemann, DLR-Standort, Göttingen, Germany, 1999, pp. 156, 157.

[7]Koppenwallner, G., Friehmelt, H., and Muller-Eigner, R., "Calibration and First Results of Redesigned Ludwieg Expansion Tube," AIAA Paper 93-5001, Nov. 1993.

[8]Funk, B. H., and Johnston, K. D., "Laser Schlieren Cross-Beam Measurements in a Supersonic Jet Shear Layer," *AIAA Journal*, Vol. 8, No. 11, 1970, pp. 2074, 2075.

[9]Garg, S., and Settles, G. S., "Unsteady Pressure Loads Generated by Swept-Shock-Wave/Boundary-Layer Interactions," *AIAA Journal*, Vol. 34, No. 6, 1996, pp. 1174–1181.

[10]Willmarth, W. W., Kuethe, A. M., and Crocker, G. H., "Stagnation Point Fluctuations on a Body of Revolution," *Physics of Fluids*, Vol. 2, No. 6, 1959, pp. 714–716.

M. Torres
Associate Editor

Modeling of Performance of an Artillery Shell Using Neural Networks

A. K. Ghosh,* S. C. Raisinghani,† and S. K. Dehury‡
Indian Institute of Technology Kanpur, Kanpur 208016, UP, India

Introduction

ARTILLERY comprises an important wing of an army in providing firepower, during both war and cross-border skirmishes with the enemy. Artillery shells are a class of projectiles around which much of aeroballistic theory was originally developed, and it continues to form a significant part of aeroballistician's interest. The performance of the artillery shell is governed by many factors, such as muzzle velocity irregularity, jump and throw off; ambient meteorological conditions such as temperature, density, head/tailwind, and crosswind; and manufacturing procedures resulting in differences in shape, size, mass, and yawing behavior. The conventional approach hitherto used for predicting behavior and performance of a projectile such as an artillery shell was via mathematical models.[1]

Beginning with the simplest, but relatively inaccurate, in-vacuo trajectory mathematical model, more and more sophisticated models of increasing accuracy, such as the point mass model, the modified point mass model, and the six-degree-of-freedom model, have been developed. However, even the best of these models have their limitations because of 1) an inability to model all of the problem variables (e.g., the initial conditions at the time of shell leaving the barrel, the jump and throw off, the variable atmospheric conditions,

Received 1 May 2001; revision received 10 February 2002; accepted for publication 18 February 2002.

*Assistant Professor, Department of Aerospace Engineering. Member AIAA.

†Professor, Department of Aerospace Engineering. Senior Member AIAA.

‡Graduate Student, Department of Aerospace Engineering.